Macromolecular Research, Vol. 11, No. 6, pp 444-450 (2003)

Self-Diffusion of Hydrophobically End-Capped Polyethylene Oxide Urethane Resin by Using Pulsed-Gradient Spin Echo NMR Spetroscopy

Jinwoo Choi and Daewon Sohn*

Department of Chemistry, Hanyang University, 17 Haengdang-dong, Seongdong-gu, Seoul 133-791, Korea

Youngil Lee*

Dongbu Research Council, 103-2 Munji-dong, Yusung-gu, Daejeon 305-380, Korea

Chaejoon Cheong

Magnetic Resonance Team, Korea Basic Science Institute, 52 Eun-dong, Daejeon 305-333, Korea

Received May 9, 2003; Revised Oct. 4, 2003

Abstract: Hydrophobically End-capped polyethylene oxide Urethane Resin(HEUR)-associating polymers, HEUR 35(8), HEUR 35(12), and HEUR 35(18), comprise a polyethylene oxide (PEO) having a molecular weight of 35,000 that is end capped with two C_8H_{17}, $C_{12}H_{25}$, and $C_{18}H_{37}$ alkyl chains, respectively. These associating polymers were synthesized by condensation reactions with polyethylene oxides and alkyl isocyanates. The self-diffusion coefficients of HEUR-associating polymers were measured in aqueous solution by pulsed-gradient spin-echo (PGSE) nuclear magnetic resonance (NMR) spectroscopy. All polymers underwent a decrease in their mean diffusion coefficients as the concentration was increased. However, the dispersion of the diffusion coefficients, β, about the mean fluctuated with changes in concentration. The large dispersion at low concentrations of HEUR 35(8) and HEUR 35(12) is related to the interaction between hydrophobic end groups, and the large dispersion at high concentrations of HEUR 35(18) is correlated with transient network formation. These results are valuable for predicting the associating mechanism of the large aggregates before and after their critical micelle concentration.

Keywords: HEUR, PGSE-NMR, CMC, hydrophobic interaction, self-diffusion.

Introduction

HEUR, hydrophobically end-capped polyethylene oxide urethane, is a water-soluble ABA type polymer surfactant containing one hydrophilic polyethylene oxide main chain and two hydrophobic end groups attached via a urethane bond. In water, the poorly soluble end groups associate to form micelle-like clusters in which both hydrophobic end groups form the core and are surrounded by a corona of soluble chains at low concentration. As with other amphiphilic polymer micelles, the chemical incompatibility of these insoluble polymer blocks drives its phase separation to overcome the free energy penalty of contacts between solvent molecules and the insoluble alkyl chains. There is a delicate balance between the driving force for micellization by hydrophobes/water contacts and the penalty paid through loop formation and chain stretching in these flower-like micelles.[1-7] These association processes are more complex than those of traditional surfactant micelles. It is the secondary association at higher concentrations where the hydrophobic chains can bridge between neighboring micellar cores and where the hydrophilic backbone chains form loops between micelles. Some research has suggested a two-step association mechanism:[6,8] primary association forming rosette-like micelles, followed by secondary association forming extended structures connected by bridging chains. The micellar cores serve as the junctions for elastically effective chains. This is essentially identical to the suggestion of Semenov *et al.*[9] At sufficiently high concentration, the flower-like micelles link into a progressively growing network that eventually spans the entire solution, forming a three-dimensional network.[6,8-12]

These polymers are used as rheology modifiers in water-born coatings such as paints and paper coatings, adhesives, in sealants, and in oil-recovery applications. When these polymers are added to water in small amounts, the viscosity greatly increases and the solution thickens. The attractive feature of these associative polymers from an industrial

*e-mail: dsohn@ihanyang.ac.kr

point of view is their viscosity profile at different shear rates, which is due to the hydrophobic groups extend into micelle structures.[13-15] The rheological properties of these polymers have been examined by a number of research groups.[16-18] At steady shear, beyond a critical shear rate, they exhibit shear thinning behavior.[19-25]

More recently, these polymers and their solutions in water have been examined by various scattering and spectroscopic techniques including dynamic and static light scattering,[3,10,26-30] small angle neutron scattering, small angle x-ray scattering,[9,29,30] static and dynamic fluorescence,[3,13,14,21,31-33] PGSE-NMR,[1,12,25,34] and viscometry.[35] Since the PGSE NMR technique was first demonstrated by Stejskal and Tanner,[36] it has become a powerful technique for studying self-diffusion in polymer systems.[37-39] The PGSE-NMR technique is particularly suited for measuring self-diffusion coefficients in HEUR associating polymers.[1,12,33,40,41] There are many factors that influence the self-diffusion of various diffusants in polymer systems. These factors are the polymer concentration, solvent, size and shape of the diffusant, temperature, G (gradient strength), δ (pulse length), Δ (diffusion time), byproduct and any interactions in the polymer networks.

Herein, we studied the effect of concentration and hydrophobic size on the self-diffusion of HEUR. We propose an association mechanism of HEUR association polymer based on the PGSE NMR data and the previous static fluorescence data of our group.[42] In this mechanism the large aggregates with extraordinarily slow diffusion appear in very dilute solution below CMC, which do not have complete phase separation to form micelles of a fixed size. Moreover, their large size distribution causes the polydispersity of the diffusion coefficients. When the polymer concentrations extend to near the CMC, the phase is shifted to well-defined micelles. Here the diffusion coefficients are monodispersive. Above the CMC, the previously reported second transition appears with polydisperse diffusion coefficients. In this PGSE-NMR experiment, we measured not only self-diffusion coefficients, but also the polydispersity of HEUR associating polymers.

Experimental

Sample Preparation. The HEUR associating polymers were synthesized by condensation reaction of polyethylene glycol and various alkyl isocyanates (octyl, dodecyl, and octadecyl isocyanate, respectively as shown in Figure 1, Aldrich), and denoted as HEUR 35(8), HEUR 35(12), and HEUR 35(18). The mixture of 3 g of polyethylene glycol (M_w = 35,000, Fluka) and 50 mL of toluene was pre-dried at 130 °C. The mixture was cooled to 80 °C, and 20 equivalences of alkyl isocyanate (Aldrich) and dibutyltin dilaurate (10 μL, Aldrich) were added. The reaction was kept at 80 °C for about 20 hrs. Excess isocyantes were quenched with 1 mL hexanol. After this solution was cooled to room temperature, the solvent was removed using a rotatory evaporator. The polymer was recrystallized several times with THF and n-hexane, then dissolved in methanol and filtered with a 0.5 μm membrane filter to remove white impurities.[13] Six different concentrations of 0.01, 0.1, 0.3, 0.5, 0.8, and 1.0 wt% in D_2O (99.9 atom%, Aldrich) were prepared.

PGSE-NMR Experiments. The self-diffusion measurements with a standard Stejskal and Tanner PGSE NMR pulse sequence, as shown in Figure 2, were carried out

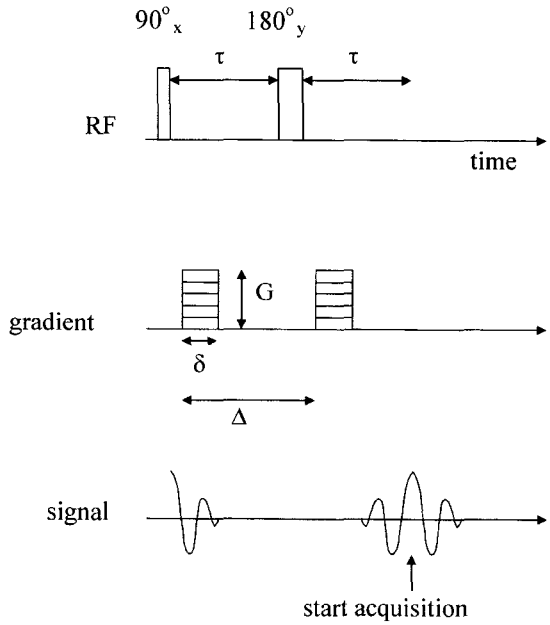

Figure 2. The pulsed-gradient spin-echo (PGSE) sequences.

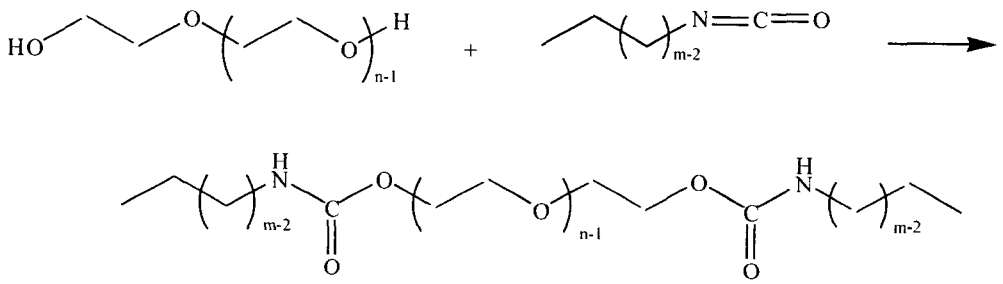

Figure 1. The structure of HEUR. n = 795 and m = 6, 10, and 16 for the HEUR 35(8), HEUR 35(12), and HEUR 35(18), respectively.

using a micro-imaging probe (model name: Micro 5) of 600 MHz Bruker DMX600 with a 14.1 Tesla magnet at the Korea Basic Science Institute. The gradient coils were actively shielded to avoid eddy current distortions of the NMR signals and their highly sophisticated designed guaranteed low inductance at very fast switching times and high gradient linearity. Their maximum gradient strength was 10 T/m. A gradient controller unit was used to generate a fast linear field gradient pulse, and a gradient blanking unit was used to separate the gradient amplifier from the gradient coil during data acquisition. A 90° pulse length of 7.6 μs was used. Four scans and two dummy scans were made. The spectral width was 10 kHz, the number of sampled points was 16 k, and the recycle delay between scans was 30 s. In this NMR study, the PGSE experiments were performed at room temperature and the axis of the magnetic field gradient was parallel to the main magnetic field. The pulsed-gradient strength G was varied from 0 to 0.1 T/m. For HEUR 35(18), the G was varied from 0 to 0.2 T/m for 0.298 and 0.517 wt% and from 0 to 0.3 T/m for 0.793 and 0.985 wt%. The field gradient strength was verified daily with a sample of 2 vol% H_2O in D_2O (1.901×10^{-9} m^2/s) of a known self-diffusion coefficient.[41] The time between the leading edges of the gradient pulses Δ and the duration of the gradient pulses δ values employed in these experiments were 250 and 40 ms, respectively. The phase correction was performed in magnitude mode for the Fourier transformed echo signal. The self-diffusion coefficient was calculated from the attenuation of the NMR signal area as a function of the gradient strength and durations.

Results and Discussion

For the PGSE NMR experiments, the sample was placed in a homogeneous magnetic field for establishing equilibrium. A radio frequency (RF) 90° pulse was applied to rotate the macroscopic magnetization of the nuclear spins into the transverse plane which is perpendicular to the main magnetic field. Subsequently, a linear field gradient pulse was imposed to label the positions of the nuclear spins. Then a second RF 180° pulse was irradiated to invert the phase of the local magnetization of the nuclear spins. Again, an identical linear field gradient pulse after second RF pulse was applied to record the spin echo. The irreversible loss of phase coherence occurred due to the diffusion of spins along the direction of the magnetic field gradient in the time span between the gradient pulses. This causes a reduction in the amplitude of spin echo which is related to the self-diffusion coefficient of the molecules for the given nuclear spin of interest. The self-diffusion coefficient was calculated from the reduction ratio of echo signal intensity (A) in the presence of gradient pulses according to the Eq. 1.[36,44]

$$A_{2\tau}/A_0 = \exp[(-(\gamma G\delta)^2)(\Delta - \delta/3) \cdot D] \quad (1)$$

where $A_{2\tau}$ is the echo intensity at time 2τ following the start of the PGSE pulse sequence, A_0 is the echo intensity in the absence of gradient pulses, γ is the gyromagnetic ratio of ^1H, and D is the self-diffusion coefficient. The experiment is usually performed under conditions of constant τ which means that the spin-spin relaxation (T_2) term $A_0 = A_{\tau=0} \exp(-2\tau/T_2)$ is constant and can be ignored. The self-diffusion coefficient can be derived from fitting of a plot of the ratio of echo signal intensity as a function of $(\gamma G\delta)^2(\Delta - \delta/3)$. Usually, a monoexponential decrease of $A_{2\tau}/A_0$ should be observed, but multiexponential decay can often be observed in polymer systems. This may make it difficult to determine the self-diffusion coefficient. The multiexponential decaying behavior of $A_{2\tau}/A_0$ is due to the heterogeneity of the polymer systems, any specific interactions with the polymers, the polydispersity of diffusants, or anomalous diffusion from intra- and intermolecular interactions.[12,33,41,43,45,46]

Figures 3, 4, and 5 show typical plots of the logarithm of the signal intensity of HEUR 35(8), HEUR 35(12), and

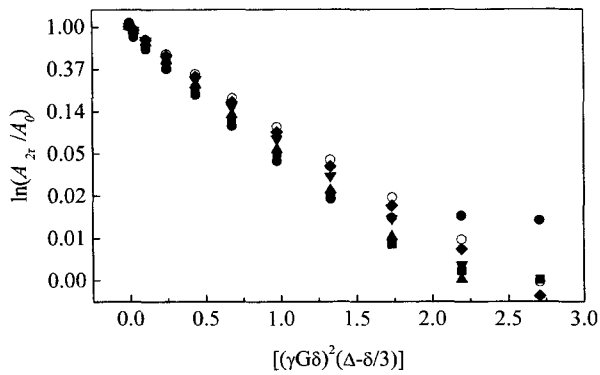

Figure 3. The logarithms of the signal intensity of the HEUR 35(8). 1.007 (○), 0.804 (◆), 0.496 (▼), 0.298 (▲), 0.098 (■), and 0.012 (●) wt%. The solid symbols show multi-exponential decays.

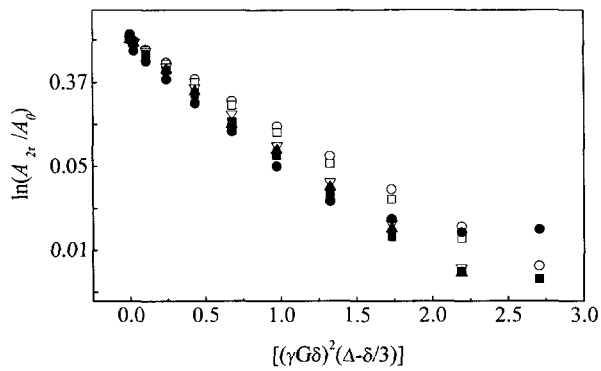

Figure 4. The logarithms of the signal intensity of the HEUR 35(12). 0.993 (○), 0.827 (□), 0.505 (▽), 0.339 (▲), 0.099 (■), and 0.012 (●) wt% The solid symbols show multi-exponential decays.

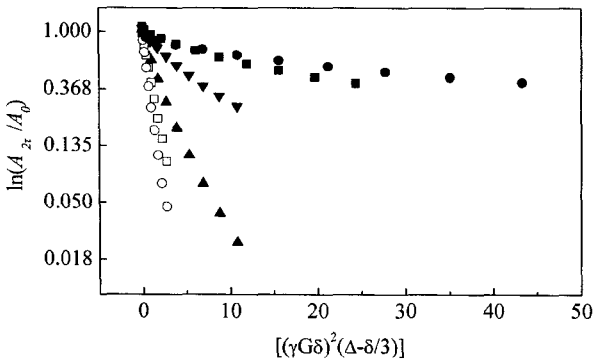

Figure 5. The logarithms of the signal intensity of the HEUR 35 (18). 0.985 (●), 0.793 (■), 0.517 (▼), 0.298(▲), 0.098(□), and 0.011 (○) wt%. The solid symbols show multi-exponential decays.

HEUR 35(18) as a function of the gradient pulse duration at various concentrations in deuterium oxide. Here we could find the breakpoint. These plots shows two different behaviors; one shows a single exponential decrease in intensity and the other shows a multi-exponential decrease. The multi-exponential decay of reduced intensity can be analyzed by a stretched exponential as described by Nyström *et al.*[47]

$$A_{2\tau}/A_0 = \exp[-(XD_e)^{\beta}] \quad (2)$$

where $X = (\gamma G\delta)^2(\Delta-\delta/3)$ and β is a parameter describing the width of the distribution of the diffusion coefficients about the mean value. The numerical range of parameter β is from 0 to 1. When $\beta = 1$, the diffusion coefficient is monodispersive. When $\beta < 1$, however, diffusion coefficients are distributed. The efficient self-diffusion D_e is used to calculate the mean diffusion coefficient, D_m, by

$$1/D_m = \int_0^{\infty} \exp[-(XD_e)^{\beta}]dX = (1/\beta)(1/D_e)\Gamma(1/\beta) \quad (3)$$

where Γ denotes the gamma function. Values for β and D_e can be estimated by plotting $\ln[\ln(A_0/A_{2\tau})]$ versus $\ln(X)$, which should be linear with a slope equal to β and an intercept equal to $\beta\ln(D_e)$. According to the previous results of our group, the CMCs were about 1, 0.5, and 0.01 wt% for HEUR 35(8), 35(12), and 35(18), respectively.[42] At these points, the β values were co-adjacent 1. The $\ln[\ln(A_0/A_{2\tau})]$ versus $\ln(X)$ plots in Figures 6, 7, and 8 compare the exponential curves with the highest and the lowest β values. HEUR 35(8) and HEUR 35(12) have β values which increase gradually from 0.678 to 0.991, and their D_e values range from 4.39×10^{-11} to 2.12×10^{-11} m²/s. However, the β values of HEUR 35(18) decrease from 0.99 to 0.505. Therefore, D_m values for HEUR 35(18) can be estimated using Eq. 3. Tables I, II, and III show the corresponding values for D_m, D_e, and β of these HEUR associating polymers.

Figures 9 and 10 compare the mean diffusion coefficients

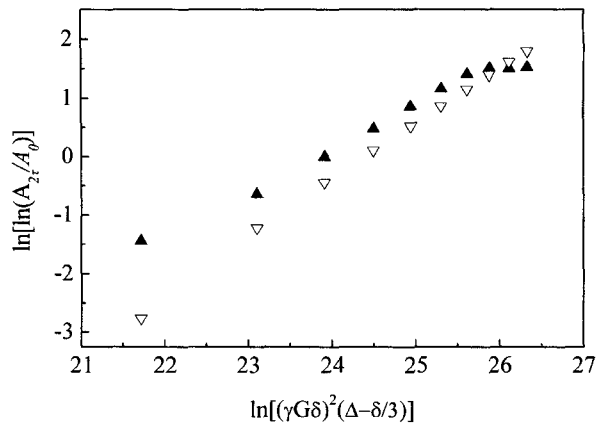

Figure 6. The double logarithms of the signal intensity of the HEUR 35(8) determining the width of the distribution of diffusion coefficients (β) and the efficient diffusion coefficients (D_e). β corresponds to the slope, and the intercept corresponds to $\beta(\ln D_e)$. 1.007(▽) and 0.012(▲) wt%.

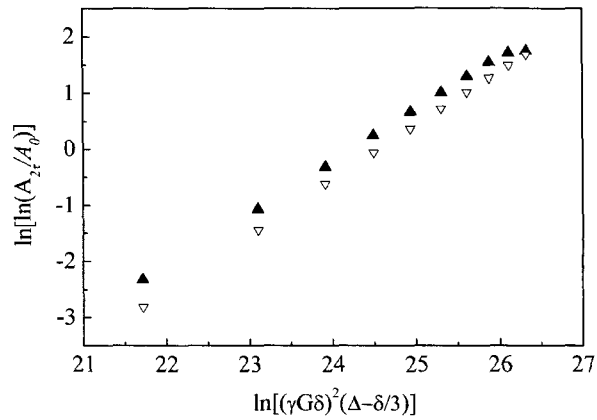

Figure 7. The double logarithms of the signal intensity of the HEUR 35(12). 0.505 (▽) and 0.011 (▲) wt%.

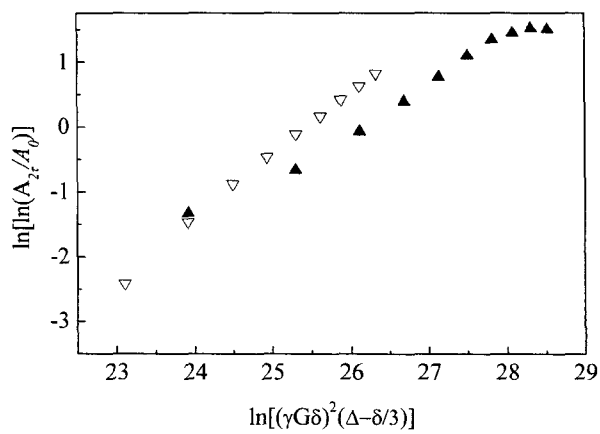

Figure 8. The double logarithms of the signal intensity of the HEUR 35(18). 0.098 (▽) and 0.985 (▲) wt% .

of the various HEUR 35s and their efficient diffusion coefficients. While the values for D_m and D_e of HEUR 35(8) and HEUR 35(12) in Figure 9 decrease slowly, those of HEUR 35(18) in Figure 10 decrease rapidly. The factors influencing the behavior of associating polymers in solution are the concentration, molecular structure, molecular weight, and hydrophobic end group. The molecular weight of hydrophilic main group and hydrocarbon number of hydrophobic end group play an important role in the entropy-enthalpy compensation in micellization. A loss of entropy occurs during back folding of hydrophilic main groups; and a gain in free energy during the association of the hydrophobic side chains with hydrophobic interactions.[40,48] So, we compared the diffusion of HEURs in fixed concentration region and with varying side groups. HEUR 35(18) has a long alkyl chain, so its phase transitions occurs quickly i.e. in low concentrations, HEUR 35(12) and HEUR 35(8), in contrast, have slow transitions. With increasing alkyl chain length, the tendencies of association increase gradually.

The hydrodynamic scaling law can be applied to the D_m of HEUR associating polymers,[34] describing the concentration and molecular weight dependence of properties in polymer solutions. The expression is shown below.

$$D_m(c) = D_0 \exp(-\alpha c^{\gamma}) \quad (4)$$

D_0 is extrapolated from the mean self-diffusion coefficients at the infinite dilute concentrations and α and γ are scaling parameters. Values for D_0 and γ increase with increasing hydrocarbon length of the hydrophobic side group. Nevertheless, the D_0 value of HEUR 35(18) has an extraordinarily large value of slow diffusion due to the excess hydrophobic interaction of long alkyl chain. Walderhaug *et al.* show that the HEURs having C_{18} and C_{16} side chains had the comparable

Table I. The Values of β, D_e, and D_m for HEUR35(8) at Various Concentrations

Concentrations (wt%)	β	D_e ($\times 10^{-11}$ m^2/s)	D_m ($\times 10^{-11}$ m^2/s)
0.012	0.700	4.435	3.503
0.098	0.917	3.230	3.100
0.298	0.948	3.074	3.001
0.496	0.971	2.964	2.728
0.804	0.959	2.633	2.585
1.007	0.978	2.450	1.019

Table II. The Values of β, D_e, and D_m for HEUR 35(12)

Concentrations (wt%)	β	D_e ($\times 10^{-11}$ m^2/s)	D_m ($\times 10^{-11}$ m^2/s)
0.012	0.678	4.393	3.361
0.099	0.913	2.946	2.822
0.339	0.960	2.782	2.732
0.505	0.991	2.555	2.546
0.827	0.986	2.248	2.235
0.993	0.978	2.119	2.099

Table III. The Values of β, D_e, and D_m for HEUR35(18)

Concentrations (wt%)	β	D_e ($\times 10^{-11}$ m^2/s)	D_m ($\times 10^{-11}$ m^2/s)
0.011	0.926	1.3420	1.2950
0.098	0.990	0.8937	0.8997
0.298	0.937	0.4287	0.4160
0.517	0.922	0.1377	0.1326
0.793	0.866	0.4159	0.0388
0.985	0.505	0.0179	0.0091

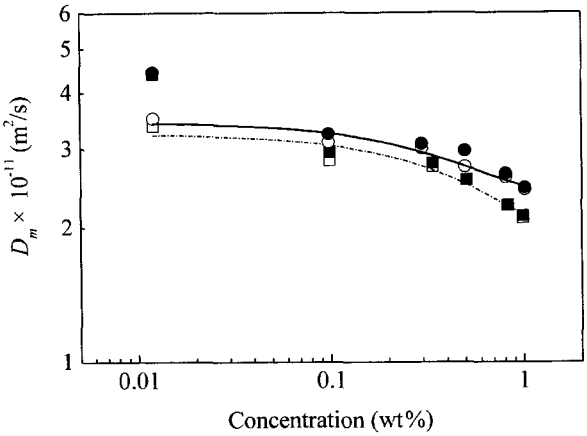

Figure 9. The D_e (solid), and D_m (open) for HEUR 35(8) (circle), and 35(12) (square).

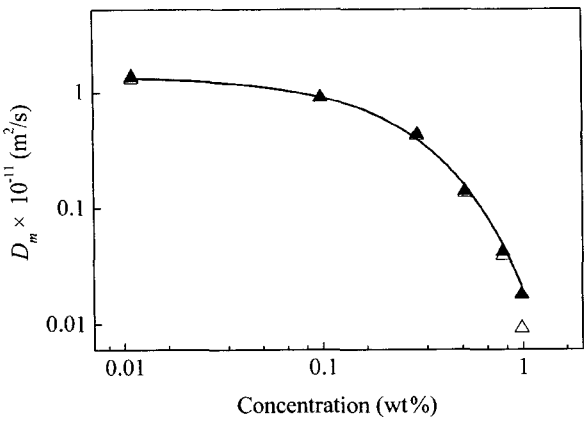

Figure 10. The D_e (△) and D_m (▲) for HEUR 35(18).

with those having shorter side groups but twice length of hydrophilic main groups.[12] Using the Stokes-Einstein relation, Eq. 5, the hydrodynamic radius (R_H) of the diffusing species depends on the self-diffusion coefficient assuming that the clusters of HEUR molecules behave as independent units in the limit of zero concentration.

$$R_H = \frac{k_b T}{6\pi\eta_0 D} \tag{5}$$

where k_b is Boltzmann's constant and η_0 is the viscosity of H_2O. The R_H values for HEUR 35(8), 35(12), and 35(18) at zero concentration were 9.91, 9.57, and 16.74 nm, respectively. Table IV summarizes the D_0, α, γ and corresponding R_H values.

As discussed above, HEUR 35(18) has phase transitions at low concentrations where the micelle and transient network appear. However, both HEUR 35(8) and HEUR 35(12) do not have the second transition.

In Figure 10, the "overlap concentration;" c^*, where D_m starts to decrease sharply is at 0.25 wt% and the corresponding diffusion coefficient, D^*, value is 4.75×10^{-12} m^2/s.

Figure 11 compares the values of β, which indicate the degree of dispersion of the diffusion coefficients, for the various HEUR 35 associating polymers over the same range of concentrations. At low concentrations, relatively short end chains HEURs, HEUR 35(8) and HEUR 35(12), have

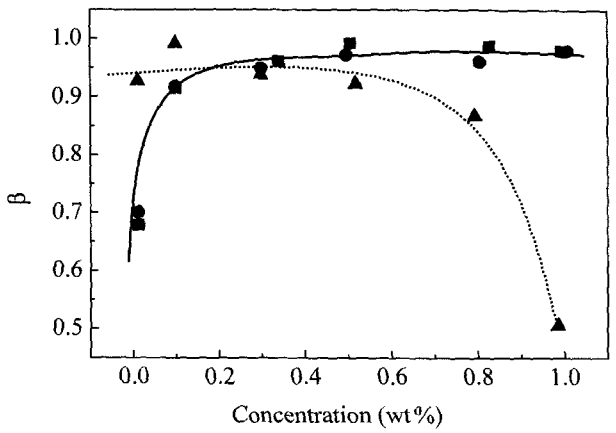

Figure 11. Distributions of diffusion coefficients about the mean values as a function of concentration. HEUR 35(8) (●), HEUR 35(12) (■), and HEUR 35(18) (▲). The lines are just for guide.

Table IV. The Values of α, γ, D_0, and R_H for HEUR35(8), HEUR35(12), and HEUR35(18)

	D_0 ($\times 10^{-11}$ m^2/s)	α	γ	R_H(nm)
HEUR 35(8)	3.44	0.350	0.734	9.9
HEUR 35(12)	3.24	0.437	0.873	9.6
HEUR 35(18)	1.92	5.212	1.019	16.7

large deviation from unity. HEUR 35(18) which has a long alkyl chain has no deviation at low concentrations, but has large deviation at high concentrations. These experimental data support the idea of the formation of intermediate structure for HEUR 35(8) and HEUR 35(12) before reach the CMC, but HEUR 35(18) maintains relatively stable micellar structure before reach the CMC. After passing through the CMC, HEUR 35(8) and HEUR 35(12) are unstable, but monodispersed structures. However, HEUR 35(18) has a stable, but polydispersed structure. The CMCs of these HEURs were additionally measured by static fluorescence.[42] They were examined by fluorescence emission spectrum of pyrene in water. Pyrene is a polar sensitive dye which can provide information about the hydrophobicity of the dye environment in the micelle. The spectrum has 5 peaks. The intensity of peak I increases with the polarity of solvent. The intensity ratio of I/III decreases steeply with micelle formation because hydrophobic pyrene is isolated in the hydrophobic core of the micelles. In Figure 11, the turning points of the value β are 1.007, 0.505, and 0.0098 wt% and these are the same values as the CMC obtained from the static fluorescence measurements. The values of β on NMR provide more information than the intensity measurement from the static fluorescence. These experimental observations enable us to determine several different stages of the micelle formation. The first stage is the formation of the "premicelle" with $\beta < 1$. There are some diffusants which have slower diffusion coefficients than the micelles, although their mean diffusion coefficients are faster. The tendency for low β values below the CMC means that there are random aggregates without whole phase separation and hydrophobic domains before micellization. Alami *et al.* referred to these models as a mixture of free polymer, oligomer, and open aggregates.[10,28] In our case, these aggregates diffuse slower from 2 to 25 times than the free polymers. The second stage is "micellization" which is the first phase transition with the culminating β values. Micelles have a fixed size and shape. The last stage is the second phase transitions in which micelles interdiffuse each other and form the larger structures without fixed form and structure. In this stage, β is lesser than 1, too. The suggested mechanism is shown in Figure 12.

We predict the associating mechanism containing the large aggregates before and after critical micelle concentration (CMC) by using PGSE-NMR which is sensitive enough to detect the diffusion of very small molecules and to distinguish free molecules, oligomers, and aggregates. We could observe the micellization and other interactions between small molecules that could not be examined by light scattering or fluorescence measurements. Conventional fluorescence technique provides the quantitative value of the critical micelle concentration, but the PGSE-NMR gives more detail information about the conformation and intermolecular interaction between the ABA type polymer surfactants.

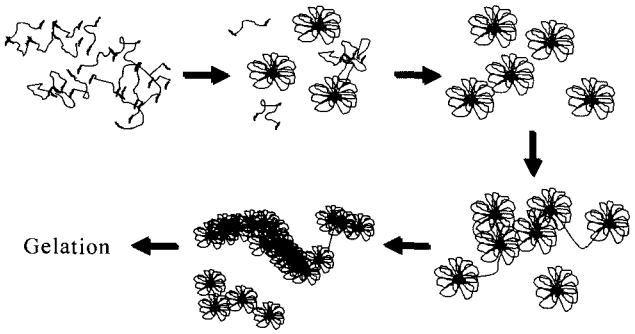

Figure 12. Schematic model of the association mechanism for HEUR associating polymers.

Acknowledgements. This work is supported by the research grant from National R & D Project for Nano Sci. Tech. (KISTEP-M10213240001-02B1524-00110), KOSEF (R-14-2002-004-01002-0), and from the Korea Institute of S & T Evaluation and Planning and the National Laboratory Program in the Ministry of Science and Technology, Korea to C.C.

References

(1) B. Rao, Y. Umera, L. Dyke, and P. M. Mcdonald, *Macromolecules*, **28**, 531 (1995).
(2) A. N. Semenov, J. F. Joanny, and A. R. Khokhlov, *Macromolecules*, **28**, 1066 (1995).
(3) E. Alami, S. A. Abrahmsen, M. Vasilescu, and M. Almgren, *J. Colloid Interf. Sci.*, **193**, 152 (1997).
(4) D. J. Lundberg, R. G. Brown, J. E. Glass, and R. R. Eley, *Langmuir*, **10**, 3027 (1995).
(5) M. J. Park, K. Char, H. D. Kim, C. H. Lee, B. S. Seong, and Y. S. Han, *Macromol. Res.*, **10**, 325 (2002).
(6) B. Xu, A. Yekta, L. Li, Z. Masoumi, and M. A. Winnik, *Collid Surface A*, **112**, 239 (1996).
(7) A. Yekta, J. Duhamel, H. Adiwidjaja, P. Brochard, and M. A. Winnik, *Langmuir*, **9**, 881 (1993).
(8) M. A. Winnik and A. Yekta, *Curr. Opin. Colloid Interface Sci.*, **2**, 424 (1997).
(9) J. Francois, S. Maitre, M. Rawiso, D. Sarazin, G. Beinert, and F. Isel, *Collid Surface A*, **112**, 251 (1996).
(10) E. Alami, M. Almgren, and W. Brown, *Macromolecules*, **29**, 2229 (1996).
(11) K. C. Tam, R. D. Jenkins, M. A. Winnik, and D. R. Bassett, *Macromolecules*, **31**, 4149 (1998).
(12) H. Walderhaug, F. K. Hasen, S. Abrahmsen, K. Persson, and P. Stilbs, *J. Phys. Chem.*, **97**, 8339 (1993).
(13) O. Vorobyova, A. Yekta, M. A. Winnik, and W. Lau, *Macromolecules*, **31**, 8998 (1998).
(14) O. Vorobyova, W. Lau, and M. A. Winnik, *Langmuir*, **17**, 1357 (2001).
(15) C. Maechling-Strasser, F. Clouet, and J. Francois, *Polymer*, **33**, 1021 (1992).
(16) Y. Morishima, *Prog. Polym. Sci.*, **15**, 949 (1990).
(17) R. D. Hester and D. R. Squir Jr., *J. Coat. Tech.*, **69**, 109 (1997).
(18) A. R. C. Baljon and T. A. Witten, *Macromolecules*, **25**, 2969 (1992).
(19) A. P. Mast, R. K. Prudhomme, and J. E. Glass, *Langmuir*, **9**, 708 (1993).
(20) R. May, P. Kaczmarski, and J. E. Glass, *Macromolecules*, **29**, 4725 (1996).
(21) B. Xu, L. Li, A. Yekta, Z. Masoumi, S. Kanagalingam, M. A. Winnik, K. Zhang, and P. M. Macdonald, *Langmuir*, **13**, 2447 (1997).
(22) J. P. Kaczmarski and J. E. Glass, *Macromolecules*, **26**, 5149 (1993).
(23) J. F. Meins and J. F. Tassin, *Macromolecules*, **34**, 2641 (2001).
(24) A. J. Reuvers, *Prog. Org. Coat.*, **35**, 171 (1999).
(25) K. Zhang, B. Xu, M. A. Winnik, and P. M. Macdonald, *J. Phys. Chem.*, **100**, 9834 (1996).
(26) E. Feitosa, W. Brown, and P. Hansson, *Macromolecules*, **29**, 2169 (1996).
(27) R. Johannsson, C. Chassenieux, D. Durand, T. Nicolai, P. Vanhoorne, and R. Jerome, *Macromolecules*, **28**, 8504 (1995).
(28) E. Alami, M. Almgren, and W. Brown, *Macromolecules*, **29**, 5026 (1996).
(29) S. Saito, S. Koizumi, K. Matsuzaka, S. Suehiro, and T. Hashimito, *Macromolecules*, **33**, 2153 (2000).
(30) C. Gourier, E. Beaudoin, M. Duval, D. Sarazin, S. Maître, and J. François, *J. Colloid Interf. Sci.*, **230**, 41 (2000).
(31) A. Yekta, J. Duhamel, P. Brochard, H. Adiwidjaja, and M. A. Winnik, *Macromolecules*, **26**, 1829 (1993).
(32) J. Duhamel, A. Yekta, Y. Z. Hu, and M. A. Winnik, *Macromolecules*, **25**, 7024 (1992).
(33) B. Richey, A. B. Kirk, E. K. Eisenhart, S. Fitzwater, and J. Hook, *J. Coat Tech.*, **63**, 31 (1991).
(34) Y. Uemura and P. M. Macdonald, *Macromolecules*, **29**, 63 (1996).
(35) Q. T. Pham, W. B. Russel, J. C. Thibeault, and W. Lau, *Macromolecules*, **32**, 2996 (1999).
(36) E. O. Stejskal and J. E. Tannner, *J. Chem. Phys.*, **42**, 288 (1965).
(37) E. D. von Meerwall, *Adv. Polym. Sci.*, **52**, 1 (1984).
(38) E. D. von Meerwall, *J. Non-Cryst Solids*, **131**, 735 (1991).
(39) T. Nose, *Annu. Rep. NMR Spectrosc.*, **27**, 217 (1993).
(40) K. Persson, S. Abrahmsen, P. Stilbs, F. K. Hansen, and H. Walderhaug, *Coll. Polym. Sci.*, **270**, 465 (1992).
(41) I. Furó, I. Iliopoulos, and P. Stilbs, *J. Phys. Chem. B*, **104**, 485 (2000).
(42) K. W. Paeng, B. S. Kim, E. R. Kim, and D. Sohn, *Bull. Korean Chem. Soc.*, **21**, 623 (2000).
(43) R. Mills, *J. Phys. Chem.*, **77**, 685 (1973).
(44) P. Stilbs, *Prog. NMR Spectrosc.*, **19**, 1 (1987).
(45) W. S. Price, *Concept Magnetic Res.*, **9**, 299 (1997).
(46) L. Masaro and X. X. Zhu, *Langmuir*, **15**, 8356 (1999).
(47) B. Nyström, H. Walderhaug, and F. K.Hansen, *J. Phys. Chem.*, **97**, 7743 (1993).
(48) L. J. Chen, S. Lin, and C. C. Huang, *J. Phys. Chem. B*, **102**, 4350 (1998).